Ceramics International 44 (2018) 16058–16061

Contents lists available at ScienceDirect

Ceramics International

journal homepage: www.elsevier.com/locate/ceramint

Short communication

Size control of CuO nanocrystals grown within TiO_2 mesopores with a simple technique

Fresnel Forcade[a], Rony Snyders[b,c,**], Bernardo González[a], Xavier Noirfalise[c], Elena Vigil[a,d,*]

[a] Materials Science and Technology Institute, University of La Habana (IMRE-UH), Cuba
[b] Chimie des Interactions Plasma-Surfaces, Center of Innovation and Research in Materials and Polymers (CIRMAP), University of Mons (UMONS), Mons, Belgium
[c] Materia Nova Research Center, Mons, Belgium
[d] Physics Faculty, University of La Habana (UH), Cuba

ARTICLE INFO

Keywords:
A. Film
B. Nanocomposite
D. CuO/TiO_2
E. Photoelectrode

ABSTRACT

An economical and scalable technique, namely a modified wet-impregnation method, has been developed in order to control the size of CuO nanocrystals grown within a nanocrystalline TiO_2 mesoporous layer. Cu (II) formate aqueous solution has been used as CuO precursor and different immersion times were experimented to decrease nanocrystal size. Synthesized nanocomposite films have been characterized using scanning electron microscopy and X-ray diffraction which reveals the nanocrystal size to depend on the immersion time. Results indicate that nanocrystals grow almost linearly for immersion time shorter than 60 min. Nanocrystal growth is not linear for a long immersion time; size increased less than 10% when the immersion time changed from one to 18 h.

1. Introduction

Nanocrystalline TiO_2 combined with CuO has been widely studied recently for the so called “water splitting” or water photolysis process. Several CuO-TiO_2 suspended-particle systems have been reported [1–4]. This combination has also been used in photoelectrodes for photoelectrochemical cells (PEC) [5–8]. In the latter, one can imagine a CuO/TiO_2 three dimensional interface and CuO nanocrystal size is an important factor that must be considered [9]. It affects the CuO/TiO_2 interface performance in different ways:

1. Light absorption by CuO plays an essential role in improving water splitting when it is added to TiO_2. CuO absorbs the visible spectrum radiation because of its energy gap. Eg = 1.2–1.5 eV is the most frequently reported range [10–17] but gap value depends on nanocrystal size and morphology [18].
2. Loss of excited carriers can be avoided by controlling nanocrystal size [19].
3. For equal CuO concentration in TiO_2, a decrease of nanocrystal size leads to an increase of internal surface and interface areas. This increases recombination losses at surface and interfacial defects.
4. Nanocrystal size also affects band alignment in heterostructures where no electric field capable of separating photon-created electron-hole pairs exists due to nano size (potential difference in the nanoparticle depletion region must be larger than kT/q [20,21]). For no band bending in the CuO/TiO_2 interface due to nanocrystal size, electrons will move from CuO to TiO_2 if they can find empty states of lower energy; that is, according to band positions relative to vacuum. Smaller CuO nanocrystals could increase the gap value and improve electron transfer probability to TiO_2.

Regarding the CuO/TiO_2 interface, discrepancies exist in the literature with respect to CB offset. Chen et al. [4] and Yu et al. [3] consider TiO_2 CB energy above that of CuO. Zhijun Li et al. [6] state that high energy photoexcited electrons in CuO are thermodynamically transferred to the CB of TiO_2; even though, CuO CB bottom is lower than that of TiO_2. On the other hand, Chiang et al. [22] and Chauhan et al. [23] study CuO photoelectrodes for water splitting. According to the CuO CB values given by these authors, excited electrons in CuO could move to empty states in the TiO_2 CB if they were in a CuO/TiO_2 interface. We recently concluded [24] that excited electrons in the CuO CB occupy levels with higher energy than empty states in TiO_2 CB for the analyzed nanocrystalline CuO/TiO_2 interface. In all cases, CB positions relative to vacuum of both, CuO and TiO_2, are not very different.

Previous analysis indicates the importance of nanocrystal size control; particularly, for the CuO/TiO_2 three dimensional interface used for

* Corresponding author at: Physics Faculty, University of La Habana (UH), Cuba.
** Corresponding author at: Chimie des Interactions Plasma-Surfaces, Center of Innovation and Research in Materials and Polymers (CIRMAP), University of Mons (UMONS), Mons, Belgium
E-mail address: evigil@fisica.uh.cu (E. Vigil).

https://doi.org/10.1016/j.ceramint.2018.05.015
Received 1 December 2017; Received in revised form 27 April 2018; Accepted 3 May 2018
Available online 04 May 2018

water splitting. Nanocrystal size determines the bandgap value, the optical absorption edge, electron-hole recombination losses, recombination in interfacial and surface defects and band positions relative to vacuum.

An economical and scalable route to fabricate PEC photoelectrodes [24] is analyzed here in order to control the size of CuO nanocrystals grown within a mesoporous TiO_2 film. Pores in a TiO_2 film are filled with Cu(II) formate aqueous solution [24]. Cu(II) formate molecules adhere to the TiO_2 during the immersion time. Afterwards, heat treatment decomposes the Cu(II) formate and CuO nanocrystals grow inside TiO_2 pores. Nanocrystal size dependence on immersion time is studied.

2. Experimental procedures

2.1. Fabrication of CuO/TiO_2 films

Single layers of mesoporous TiO_2 were prepared using TiO_2 nanopowder Degussa P25 (nanocrystal mean diameter ca. 25 nm) and the well-known "doctor blade" technique developed for DSSC [25]. Air drying of the TiO_2 layer was followed by heat treatment in air at 450 °C during one hour. After cooling, the porous TiO_2 films were immersed in a 160 mM Cu (II) formate aqueous solution during a specific time. Precursor molecules should move easily through the mesoporous structure and penetrate pores [24]. Cu (II) formate adheres to the TiO_2 internal surface during the immersion time [24]. Once immersion finished, care was taken to remove the precursor solution from the sample surface so that it only remained inside the pores [24]. Samples were heat treated in air at 500 °C during three hours to guarantee complete synthesis of CuO. Water evaporates and Cu (II) formate decomposes when samples are heat treated in air [24].

2.2. Characterization

The phase identification of the films was performed by X-ray diffraction (XRD) with an Empyrean Panalytical apparatus in the range $10° < 2\theta < 60°$. Cu Kα radiation ($\lambda = 1.5406$ Å) was used for all X-ray diffraction experiments, as well as, 0.5° grazing angle. The Panalytical software for XRD HighScore version 3.0 (2012) was used for XRD pattern analysis. Scanning electron microscopy (SEM) was conducted with a Hitachi SU8020 scanning electron microscope.

3. Results and discussion

Sample types are shown in Table 1. Their names identify precursor concentration and immersion time.

Fig. 1 shows SEM cross-section images of samples 160F_18h, 160F_1h and 160F_1min where the porous morphology of the films can be appreciated. Pores are required for penetration of the hole conducting medium and performance of the three dimensional interface.

XRD patterns corresponding to samples 160F_18h, 160F_1h and 160F_1min are shown in Fig. 2. XRD line pattern is also shown for comparison (ICDD 01-080-1916). Only two CuO peaks are observed because of the low CuO concentration and its nanocrystalline character. The peak at $2\theta = 38.7°$, tenorite plane (111), is hardly resolved from an anatase peak. Therefore, peak at $2\theta = 35.5°$, tenorite plane ($\bar{1}11$), was used to obtain the values of the full width at half maximum, FWHM.

Table 1
Analyzed samples.

Sample name	Immersion time (h)	FWHM (degrees)	Crystallite size (nm)
160F_18h	18	0.303	32
160F_1h	1	0.328	25
160F_1min	1/60	0.463	18

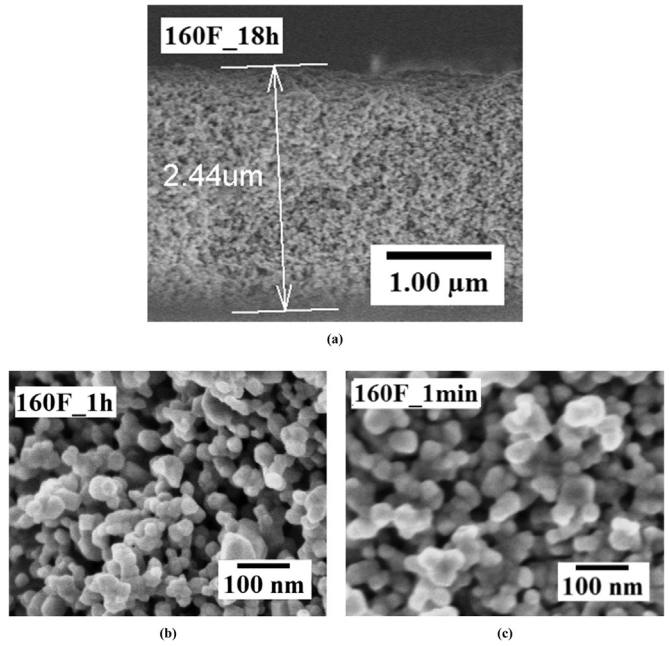

Fig. 1. SEM images of the cross-section of samples fabricated by the modified wet-impregnation technique for different immersion times: (a) 18 h, (b) 1 h and (c) 1 min.

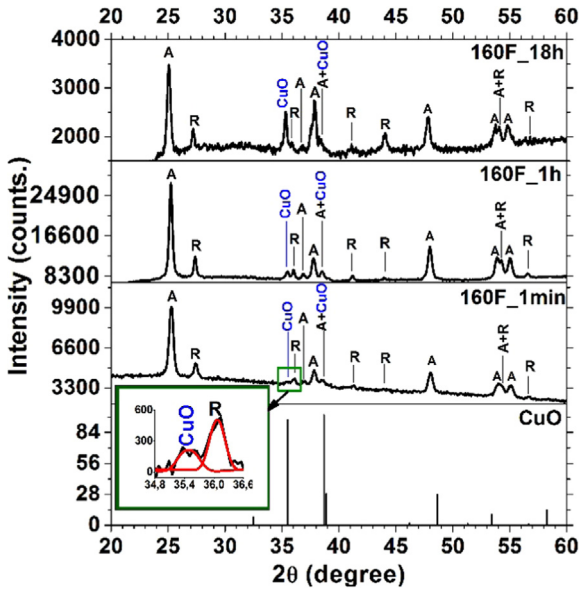

Fig. 2. CuO/TiO_2 films diffraction patterns corresponding to different immersion time together with the CuO reference pattern (ICDD 01-080-1916). A and R refer to anatase and rutile peaks, respectively. Insert: CuO peak deconvolution used to find FWHM of sample 160F_1min. The black line corresponds to experimental data and the red line shows peak deconvolution. (For interpretation of the references to color in this figure legend, the reader is referred to the web version of this article.).

Deconvolution of diffraction patterns was performed using OriginPro2015 in the interval $35° < 2\theta < 36.5°$. As an example, deconvolution for sample 160F_1min which has the lowest immersion time (therefore, lowest CuO concentration) is inserted in Fig. 2. FWHM values corresponding to $2\theta = 35.5°$ are shown in Table 1. Crystallite size was determined using Scherrer formula [26]:

$$S = \frac{K*\lambda}{FWHM*\cos\theta} \quad (4)$$

where K is a constant that depends on different factors such as the shape of the crystallite and its size distribution [26]. Spherical crystals are assumed, as well as, K = 0.90 [27]. λ is the wavelength of the X-ray radiation used (λ = 1.5406 Å) and θ is the Bragg angle. FWHM values are expressed in radians.

According to observed nanocrystals in Fig. 1, crystallite values reported in Table 1 are of the same order of magnitude. It can be shown that no band bending will occur for these values. For bulk materials, band bending and the corresponding electric field in the heterojunction depletion region are responsible for electron-hole pair separation. But Curran and Lamouche [20] calculated the minimum value of the potential difference Δφ which is able to separate charges in the depletion region. It is given by the relation 2kT/q which, for room temperature (T = 27 °C = 300 K), has an approximate value of 52 mV. Also, according to L. M. Peter [21], if the potential difference Δφ is smaller than kT/q, it has a negligible effect on charge distribution, i.e., charges in the depletion region will not be separated by the correspondingly small electric field.

For spherical particles, potential difference in the depletion region is given by the expression [28]:

$$\Delta\varphi = \frac{kT}{6q}\left(\frac{R}{L_D}\right)^2 \tag{5}$$

where L_D is the Debye length and q is the electron charge. The Debye length L_D is given by [28]:

$$L_D = \left(\frac{\epsilon_0 \epsilon kT}{2q^2 N_I}\right)^{1/2} \tag{6}$$

where ϵ_0 is the vacuum permittivity, ϵ the static dielectric constant of the material and N_I is the concentration of donors or acceptors.

Using expressions (5) and (6), it is possible to calculate the potential drop for a spherical CuO nanoparticle with radius R = 15 nm, ϵ_{CuO} = 12 [29] and $N_A = 7 \times 10^{16}$ cm^{-3} [30,31] the potential drop is Δφ = 8 mV. It will be even less for nanocrystals with a smaller size. Therefore, for previously calculated values of Δφ, charges will not be separated by the electric field in the depletion region. When the potential drop is not enough to separate photon-created electron-hole pairs, electrons will move from one semiconductor to the other if they can find empty states of lower energy. That is, band positions relative to vacuum of each semiconductor will determine thermodynamic charge transfer. If photons excite electrons in the narrow gap semiconductor of a heterostructure, these electrons will only move to the higher energy gap semiconductor if its CB bottom has a lower energy, i.e., they can only move by losing part of the energy given by the absorbed photons. Additionally, it must be mentioned that for nanocrystals with different shapes but small enough dimensions in one or more directions, bandgap increases [32–34]

Fig. 3a shows crystallite diameter vs immersion time (see Table 1). An almost linear dependence is observed for shorter times for which there are no nanoparticles at t = 0, as expected. But nanocrystal diameter for t = 18 h shows that growth rate decreases with time. This can be explained since the growth of Cu(II) formate nanocrystals inside the pores lowers the solution concentration. Also the volume occupied by the solution decreases. Therefore, considering that initially Cu(II) formate nucleates on TiO_2 but then molecules bind to Cu(II) formate rather than to TiO_2, the mass growth rate for each nanocrystal can be expressed as:

$$\frac{dm}{dt} = C - \frac{m}{\tau} \tag{7}$$

The solution of this Eq. (7) is:

$$m(t) = C\tau\left[1 - \exp\left(-\frac{t}{\tau}\right)\right] \tag{8}$$

which describes the evolution of a Cu(II) formate nanoparticle mass as a function of immersion time t. Cu(II) formate nanoparticle mass must be proportional to CuO nanoparticle mass after heat treatment. Assuming this and since CuO mass density is constant, the mass dependence of a spherical CuO nanoparticle is also given by expression (8) (values of C and τ will be different, of course). This dependence is plotted in Fig. 3b which also shows that the experimental points follow this dependence. Nanoparticle mass is practically constant for $t \gg \tau$. However, for small values of t, $\exp\left(-\frac{t}{\tau}\right) \approx 1 - \frac{t}{\tau}$ and expression (8) approximates to the linear dependence m(t) = Ct.

4. Conclusions

CuO particles in the CuO/TiO_2 composite are nanocrystalline when the modified wet-impregnation technique is used with 160 mM Cu (II) formate as precursor. The XRD analyses indicate that the size of the CuO nanocrystals decreases with decreasing immersion time. Applying the Scherrer formula, CuO nanocrystal sizes are 32 nm, 25 nm and 18 nm for immersion times of 18 h, 1 h and 1 min, respectively. The mass dependence of CuO nanocrystals on the immersion time shows that it grows almost linearly for t < 60 min, while the mass hardly changes for t > 6 h.

Acknowledgements

The authors acknowledge the support of the WBI (Fédération Wallonie-Bruxelles) for the financial support through the project SUB/2012/86559 as well as the Belgian Government (Belspo) through the "Pôle d'attraction interuniversitaire" (PAI, P07/14, "Plasma-Surface Interaction", ψ).

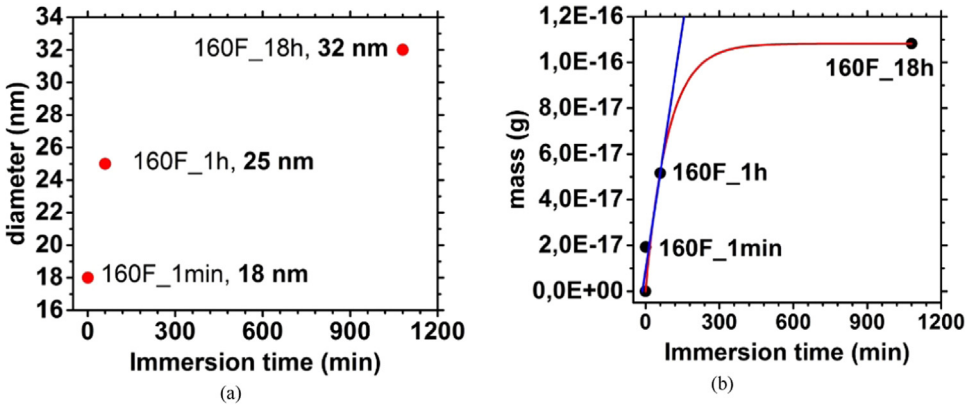

Fig. 3. (a) Crystallite diameter vs immersion time. (b) Evolution of nanoparticle mass with immersion time: experimental values (black dots) and expression (8) (red curve). (For interpretation of the references to color in this figure legend, the reader is referred to the web version of this article.).

References

[1] J. Bandara, C.P.K. Udawatta, C.S.K. Rajapakse, Highly stable CuO incorporated TiO_2 catalyst for photocatalytic hydrogen production from H_2O, Photochem. Photobiol. Sci. 4 (11) (2005) 857–861.

[2] S. Xu, A.J. Du, J. Liu, J. Ng, D.D. Sun, Highly efficient CuO incorporated TiO_2 nanotube photocatalyst for hydrogen production from water, Int. J. Hydrog. Energy 36 (11) (2011) 6560–6568.

[3] J. Yu, Y. Hai, M. Jaroniec, Photocatalytic hydrogen production over CuO-modified titania, J. Colloid Interface Sci. 357 (1) (2011) 223–228.

[4] W.T. Chen, V. Jovic, D. Sun-Waterhouse, H. Idriss, G.I.N. Waterhouse, The role of CuO in promoting photocatalytic hydrogen production over TiO_2, Int. J. Hydrog. Energy 38 (35) (2013) 15036–15048.

[5] M. Tripathi, K. Pandey, S.D. Kumar, Surface modification of semiconductor photoelectrode for improved solar cell performance, Sol. Energy Mater. Sol. Cells 91 (18) (2007) 1663–1668.

[6] Z. Li, Y. Qu, G. He, M. Humayun, S. Chen, L. Jing, Enhanced visible-light activities for PEC water reduction of CuO nanoplates by coupling with anatase TiO2 and mechanism, Appl. Surf. Sci. 351 (2015) 681–685.

[7] M. Tripathi, P. Chawla, Optimization of semiconductor ns-TiO_2-CuO admixed photoelectrode for photoelectrochemical solar cell in regard to hydrogen production, Int. J. Hydrog. Energy 41 (19) (2016) 7993–7996.

[8] S. Zhang, X.B. Cao, J. Wu, L.W. Zhu, L. Gu, Preparation of hierarchical CuO@TiO2 nanowire film and its application in photoelectrochemical water splitting, Trans. Nonferrous Met. Soc. China 26 (8) (2016) 2094–2101.

[9] A.S. Zoolfakar, R.A. Rani, A.J. Morfa, A.P. O'Mullane, K. Kalantar-Zadeh, Nanostructured copper oxide semiconductors: a perspective on materials, synthesis methods and applications, J. Mater. Chem. C 2 (27) (2014) 5247–5270.

[10] F.P. Koffyberg, F.A. Benko, A photoelectrochemical determination of the position of the conduction and valence band edges of p-type CuO, J. Appl. Phys. 53 (2) (1982) 1173–1177.

[11] K. Nakaoka, J. Ueyama, K. Ogura, Photoelectrochemical behavior of electrodeposited CuO and Cu2O thin films on conducting substrates, J. Electrochem. Soc. 151 (10) (2004) C661–C665.

[12] C.Y. Chiang, K. Aroh, N. Franson, V.R. Satsangi, S. Dass, S. Ehrman, Copper oxide nanoparticle made by flame spray pyrolysis for photoelectrochemical water splitting - Part II. Photoelectrochemical study, Int. J. Hydrog. Energy 36 (24) (2011) 15519–15526.

[13] V. Dhanasekaran, T. Mahalingam, Electrochemical and Physical Properties of Electroplated CuO thin films, J. Nanosci. Nanotechnol. 13 (1) (2013) 250–259.

[14] A.H. Alami, A. Allagui, H. Alawadhi, Microstructural and optical studies of CuO thin films prepared by chemical ageing of copper substrate in alkaline ammonia solution, J. Alloy. Compd. 617 (2014) 542–546.

[15] R. Khan, M. Vaseem, L.W. Jang, J.H. Yun, Y.B. Hahn, I.H. Lee, Low temperature preparation of CuO nanospheres and urchin-shaped structures via hydrothermal route, J. Alloy. Compd. 609 (2014) 211–214.

[16] C.R. Gobbiner, A.V.M. Ali, D. Kekuda, CuO/ZnO planar bilayer heterojunction grown by reactive dc magnetron sputtering, J. Mater. Sci. Mater. Electron. (2015) 9801–9807.

[17] M.J. Hong, Y.C. Lin, L.C. Chao, P.H. Lin, B.R. Huang, Cupric and cuprous oxide by reactive ion beam sputter deposition and the photosensing properties of cupric oxide metal-semiconductor-metal Schottky photodiodes, Appl. Surf. Sci. 346 (2015) 18–23.

[18] Q. Zhang, K. Zhang, D. Xu, G. Yang, H. Huang, F. Nie, C. Liu, S. Yang, CuO nanostructures: synthesis, characterization, growth mechanisms, fundamental properties, and applications, Prog. Mater. Sci. 60 (1) (2014) 208–337.

[19] A. Hagfeldt, M. Graetzel, Light-induced redox reactions in nanocrystalline systems, Chem. Rev. 95 (1) (1995) 49–68.

[20] J.S. Curran, D. Lamouche, Transport and kinetics in photoelectrolysis by semiconductor particles in suspension, J. Phys. Chem. 87 (26) (1983) 5405–5411.

[21] L.M. Peter, Chapter 1 - Photoelectrochemistry: from basic principles to photocatalysis, in: J. Schneider, D. Bahnemann, J. Ye, G.L. Puma, D.D. Dionysiou (Eds.), Photocatalysis: Fundamentals and Perspectives, Royal Society of Chemistry, 2016, pp. 3–28.

[22] C.Y. Chiang, Y. Shin, K. Aroh, S. Ehrman, Copper oxide photocathodes prepared by a solution based process, Int. J. Hydrog. Energy 37 (10) (2012) 8232–8239.

[23] D. Chauhan, V.R. Satsangi, S. Dass, R. Shrivastav, Preparation and characterization of nanostructured CuO thin films for photoelectrochemical splitting of water, Bull. Mater. Sci. 29 (7) (2006) 709–716.

[24] F. Forcade, R. Snyders, G. Guisbiers, B. Gonzalez, X. Noirfalise, E. Vigil, Impact of the chemical precursor on the crystalline constitution of nano-CuO/TiO_2 films, Mater. Res. Bull. 70 (2015) 248–253.

[25] G.P. Smestad, M. Grätzel, Demonstrating electron transfer and nanotechnology: a natural dye-sensitized nanocrystalline energy converter, J. Chem. Educ. 75 (6) (1998) 752–756.

[26] J.I. Langford, A. Wilson, Scherrer after sixty years: a survey and some new results in the determination of crystallite size, J. Appl. Crystallogr. 11 (2) (1978) 102–113.

[27] H.P. Klug, L.E. Alexander, X-Ray Diffraction Procedures, in: Wiley-Interscience (Ed.) X-Ray Diffraction Procedures, 1974, pp. 656, 687.

[28] C.A. Grimes, O.K. Varghese, S. Ranjan, Light, Water, Hydrogen The Solar Generation of Hydrogen by Water Photoelectrolysis, Springer, US, 2008.

[29] W.Y. Ching, Y.N. Xu, K.W. Wong, Ground-state and optical properties of Cu2O and CuO crystals, Phys. Rev. B 40 (11) (1989) 7684–7695.

[30] A.H. Jayatissa, K. Guo, A.C. Jayasuriya, Fabrication of cuprous and cupric oxide thin films by heat treatment, Appl. Surf. Sci. 255 (23) (2009) 9474–9479.

[31] T. Dimopoulos, A. Peić, P. Müllner, M. Neuschitzer, R. Resel, S. Abermann, M. Postl, E.J.W. List, S. Yakunin, W. Heiss, H. Brückl, Photovoltaic properties of thin film heterojunctions with cupric oxide absorber, J. Renew. Sustain. Energy 5 (1) (2013) (011205-011201–011205-011211).

[32] B. Enright, D. Fitzmaurice, Spectroscopic determination of electron and hole effective masses in a nanocrystalline semiconductor film, J. Phys. Chem. 100 (3) (1996) 1027–1035.

[33] S. Rühle, M. Shalom, A. Zaban, Quantum-dot-sensitized solar cells, ChemPhysChem 11 (11) (2010) 2290–2304.

[34] H. Zheng, J.Z. Ou, M.S. Strano, R.B. Kaner, A. Mitchell, K. Kalantar-Zadeh, Nanostructured tungsten oxide - properties, synthesis, and applications, Adv. Funct. Mater. 21 (12) (2011) 2175–2196.